

Regional Attention with Architecture-Rebuilt 3D Network for RGB-D Gesture Recognition

Benjia Zhou¹, Yunan Li^{3,4,*}, Jun Wan^{2,5†}

¹ Macau University of Science and Technology, Macau SAR, China

² National Laboratory of Pattern Recognition, Institute of Automation, Chinese Academy of Sciences, Beijing, China

³ School of Computer Science and Technology, Xidian University, China

⁴ Xi'an Key Laboratory of Big Data and Intelligent Vision, China

⁵ School of Artificial Intelligence, University of Chinese Academy of Sciences, Beijing, China

19098536ii20001@student.must.edu.mo, yunanli@xidian.edu.cn, jun.wan@ia.ac.cn

Abstract

Human gesture recognition has drawn much attention in the area of computer vision. However, the performance of gesture recognition is always influenced by some gesture-irrelevant factors like the background and the clothes of performers. Therefore, focusing on the regions of hand/arm is important to the gesture recognition. Meanwhile, a more adaptive architecture-searched network structure can also perform better than the block-fixed ones like Resnet since it increases the diversity of features in different stages of the network better. In this paper, we propose a regional attention with architecture-rebuilt 3D network (RAAR3DNet) for gesture recognition. We replace the fixed Inception modules with the automatically rebuilt structure through the network via Neural Architecture Search (NAS), owing to the different shape and representation ability of features in the early, middle, and late stage of the network. It enables the network to capture different levels of feature representations at different layers more adaptively. Meanwhile, we also design a stackable regional attention module called dynamic-static Attention (DSA), which derives a Gaussian guidance heatmap and dynamic motion map to highlight the hand/arm regions and the motion information in the spatial and temporal domains, respectively. Extensive experiments on two recent large-scale RGB-D gesture datasets validate the effectiveness of the proposed method and show it outperforms state-of-the-art methods. The codes of our method are available at: <https://github.com/zhoubenjia/RAAR3DNet>.

Introduction

Gesture is produced as part of deliberate action and signs, involving the motion of the up body, especially the arms, hands, and fingers. Video-based classification makes an essential component in gesture recognition. It has been applied to many human-centred tasks, such as apparent personality analysis (Li et al. 2020), sign language recognition (Cui, Liu, and Zhang 2019) and human-computer interaction

(HCI) (Wang et al. 2016b). The handcrafted features (Wan, Guo, and Li 2015) are always used for gesture recognition in the early years. The powerful feature representation ability of deep learning also promotes the application of neural networks in the field of gesture recognition (Karpathy et al. 2014; Li et al. 2016; Miao et al. 2017; Simonyan and Zisserman 2014; Narayana, Beveridge, and Draper 2018).

For most of the deep learning-based gesture recognition methods, some popular networks like ResNet (He et al. 2016), SENet (Hu, Shen, and Sun 2018) and Inflated 3D Network (I3D) (Carreira and Zisserman 2017) are usually employed as the backbone for gesture recognition. Although these networks have achieved great success in many tasks, it is still worth pointing that the same modules are shared from shallow to deep layers in these networks. Even the modules in networks like I3D that employ multi-branch structure to improve the width and diversity are fixed and all the same through the network. However, features in the early stage and late stage are quite different. Features in the early stage are low-level features, which show the visual texture in each frame, whereas the high-level features in the late stage are abstracted and more related to the class of gestures. Therefore, it is not suitable to use the same structure to learn different features, and then we need to make the network more adaptive and automatically determine what the shape is for different parts of it.

Meanwhile, one of the most significant challenges hindering the improvement of recognition accuracy is the influence of gesture-irrelevant factors, such as backgrounds, different clothes of performers, and so on. The various textures and appearances could mislead the network to learn inconsequential or less important features. For dynamic gesture recognition from a video sequence, we believe it is vital to focus on gesture movements, such as hands, arms or elbows of the performers. Many researchers notice that it is critical to make the network focusing on the gesture regions both spatially and temporally. Modules such as hand detector (Wang et al. 2016c; Liu et al. 2017), and additional modalities of data like optical flow (Li et al. 2017) or saliency (Li et al. 2018) are widely used via combining with the raw RGB (and depth) data to design different algorithms. However, most of them require extra offline oper-

*Benjia Zhou and Yunan Li contribute equally to this paper.

†Corresponding author; This work was done by Benjia Zhou who visited the lab of Center for Biometrics and Security Research, NLPR, CASIA.

Copyright © 2021, Association for the Advancement of Artificial Intelligence (www.aaai.org). All rights reserved.

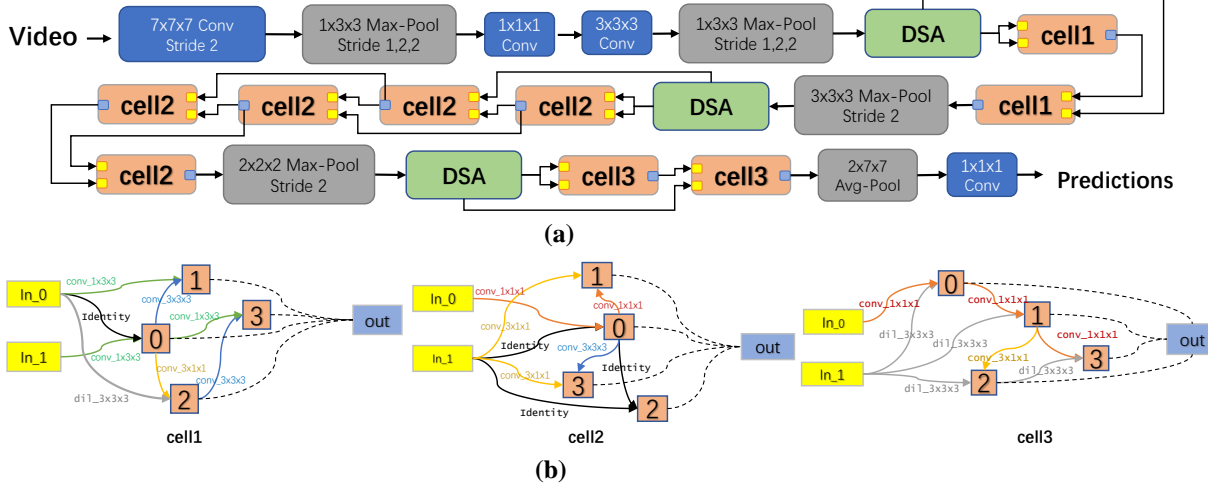


Figure 1: The pipeline of the proposed method. (a) the structure of the entire RAAR3DNet. (b) the inner structure of automatically rebuilt cell1, cell2, and cell3. Each cell is composed of two input nodes, four intermediate nodes and one output node. The output node is obtained by combining features from intermediate nodes with some reduction operation (e.g., concatenation), which are marked as the dashed lines in (b). We take the I3D network as the backbone, and utilize NAS to automatically rebuild the structure of Inception Modules in it. The reconstructed network shows different structure to fit multi-scale features. Cell1 and cell2, which are in the early and middle stage of the network, tend to employ convolution kernels with small receptive fields to capture the low-level texture features more easily, whereas cell3s at the end of the network perform dilated convolution operations to capture the more abstract and semantically high-level features.

ations (e.g., hand detection, optical flow calculation) in advance. It would increase time complexity because of using hand detector network in the testing stage. Therefore, it may be more reasonable if the attention maps of gesture regions are learned along with the task of gesture recognition in the same network.

Inspired by the above discussions, we propose a regional attention with architecture-rebuilt 3D network for dynamic gesture recognition based on RGB-D data, which is illustrated in Fig.1. We take the I3D¹ network as the backbone and employ the theory of NAS to find the optimal combination of different operations in each module of the network. To make the network focus on the gesture regions, we propose a regional attention module DSA, which includes a static attention sub-module (SAtt) and dynamic attention sub-module (DAtt). For static attention, we learn a heatmap of hands or body for each frame with the supervision of the Gaussian map of skeleton keypoints. It indicates where the hands/arms are and highlights these regions. For dynamic attention, we present a fast approximate rank pooling algorithm to learn the accumulated dynamic images, which reduces the time complexity a lot when compared with the traditional rank pooling techniques (Bilen et al. 2016, 2017) and thus can give a real-time dynamic image computation. Then with the DSA structure applied, the network can pay attention to the gesture regions spatiotemporally. Our contri-

butions can be summarized as three-fold:

(1) We replace the structure-fixed modules in the general network with automatically reconstructed cells via NAS. The cells in the early, middle, and late stages of the network can have different structures and learn the low-level and high-level features more adaptively.

(2) We propose a stackable attention structure, called DSA, to generate attention map in both spatial and temporal space. DSA consists of the SAtt and DAtt sub-modules. SAtt highlights the hands/arms features via an online learnable Gaussian skeleton heatmap while DAtt captures the gesture motions via the proposed fast approximate rank pooling algorithm with decreasing the time complexity to a large extent.

(3) Extensive experiments that prove the integration of our designs can ultimately improve the performance of gesture recognition. Experiments demonstrate that our method can strike the balance between good performance and low computation burden, and outperform those top techniques on two large-scale gesture datasets.

Related Work

Evolution of Approaches for Gesture Recognition

The study on gesture taxonomies and representations has been continued for many years. Early methods are often based on handcrafted features (Klaser, Marszalek, and Schmid 2008; Wan et al. 2014). Recently, the rapid progress of deep learning boosts many deep neural network-based

¹We still utilize a two-stream configuration - with one I3D network trained on RGB inputs, and another on depth inputs.

feature extraction methods. The 2D convolutional neural network (CNN) and its derivations combining different branches for RGB and optical flow data (Simonyan and Zisserman 2014) are first used for gesture/action recognition tasks. Then some works (Tran et al. 2015; Li et al. 2017; Carreira and Zisserman 2017) use the 3D CNN for recognizing gestures, whereas some other methods (Zhu et al. 2017; Zhang et al. 2018) employ LSTM and its variants to model the temporal relationships for the gestures. There are also some methods (Wang et al. 2016b, 2018) exploited the features like dynamic images instead of the raw RGB-D data and used them as the inputs for gesture recognition. Besides the RGB-D data, some other modalities of data like optical flow (Li et al. 2018; Miao et al. 2017) or saliency video (Li et al. 2017; Duan et al. 2018) are also employed for improving the performance.

Neural Architecture Search in Action Recognition

Our work is driven by Neural Architecture Search (NAS) (Liu, Simonyan, and Yang 2019; Xu et al. 2019). The development of NAS can be summarized in three branches: 1) based on reinforcement learning (Zoph et al. 2018), 2) based on evolution (Real et al. 2019, 2017) and 3) based on gradient (Liu, Simonyan, and Yang 2019; Xu et al. 2019). Thanks to the recent high-efficiency and high-precision search methods of NAS, many NAS-based single-modal and multi-modal methods have been applied in action and gesture recognition tasks (Zhang et al. 2020; Yu et al. 2020). Peng et al. (Peng, Hong, and Zhao 2019) first attempted to automatically design a neural network for video action recognition tasks through NAS. At the same time, in order to reduce search costs, they introduced a temporal segmentation method that reduced the computational cost without losing global video information. Qiu et al. (Qiu, Yao, and Mei 2017) proposed Scheduled Differentiable Architecture Search (DAS), which can efficiently and automatically explore the network structure through gradient descent in images and videos. Pérez-Rúa et al. (Pérez-Rúa et al. 2019) proposed a general multi-modal neural architecture search method (MFAS), which solved the problem of finding a good architecture for multi-modal classification problems. Wang et al. (Wang et al. 2020) propose a novel search space for spatiotemporal attention cells (AttentionNAS) for video classification tasks. Different from the work of others, we utilize NAS to make the network automatically rebuild the structure of modules in the I3D to capture different levels of feature representations at different layers more adaptively.

Attention Mechanism in Gesture Recognition

Attention mechanism has been wildly used in both low-level and high-level tasks like pose estimation (Chu et al. 2017), object detection (Li et al. 2019a) and image restoration (Li et al. 2019b). As the interference of backgrounds, the clothes of performers and the diversity of presentation for the same gesture are still the barrier for improving the recognition accuracy, many researchers also employ the attention mechanism to guide the network to focus on the gesture itself through the video. Some methods concentrate on the regions

of gesture in each frame. Liu et al. (Liu et al. 2017) leverage the faster R-CNN (Ren et al. 2015) as the hand detector to highlight the corresponding regions. Lin et al. (Lin et al. 2018) utilize both detected hands and skeleton information to further focus on the gesture. The work (Narayana, Bevridge, and Draper 2018) uses a focus of attention network (FOANet) to extract global raw data, local left and right hand regions via different networks. The other ones mainly concern about the motion information among frames. In (Li et al. 2018; Miao et al. 2017), the additional modality of optical flow data is used to capture the movements in videos. Zhang et al. (Zhang et al. 2018) explore attention modules used in different gates of the LSTM when incorporating it and the 3D CNNs (Tran et al. 2015). Although with these techniques the network can focus on the gestures, extra modalities of data served as an input of the network or offline training process for models like hand detector are always inevitable. On the contrary, the attention module of DSA in our method does not require any other data except for the RGB-D ones from the original dataset. The module can also be learned end-to-end within the recognition network, and it makes the network easier to apply to different situations with less time complexity. Meanwhile, since the DSA highlights both body parts in each frame and the movements through the adjacent frames, it facilitates the advantage of the temporal and spatial attention concurrently.

Proposed Method

Overview of the network

The pipeline of RAAR3DNet is shown in Fig.1. The network takes the I3D network as the backbone, and leverages NAS to automatically find the optimal structure for early, middle and late stage of the network to replace the original shape-fixed Inception Modules. Meanwhile, to better focus on the location and movement information of gesture-related parts like hands and arms, as show in Fig.2, a stackable regional attention module DSA is embedded in the network.

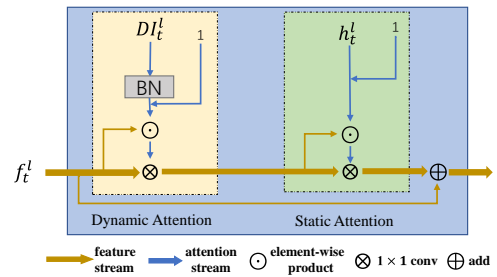


Figure 2: The detail of DSA module. It has two sub-modules of dynamic attention (DAtt) and static attention (SAtt), which are sequentially combined together.

Local Network Structure Search in I3D

We use PC-darts (Xu et al. 2019), which based on gradient descent and more efficient than darts (Liu, Simonyan, and Yang 2019), to search more efficient architecture for gesture

recognition. In the search stage, we search and rebuild more adaptively structures and replace the Inception Modules in the I3D network with them. As shown in Fig.1, because the features in different stages of the backbone have different solutions, we design three kinds of cells to learn the different levels of features. Specifically, we replace the first two Inception Modules in the I3D with **cell1**, the middle five Inception Modules with **cell2**, and the last two Inception Modules with **cell3**. Each cell represents a directed acyclic graph (DAG) with k nodes $\{m_i\}_{i=0}^{k-1}$. Each node indicates an output of a network layer, and each edge (i, j) of the DAG indicates the information flow from node m_i to m_j , which consists of the candidate operations weighted by the architecture parameter $\alpha^{(i,j)}$. Different from the I3D network which only employ three operation 'Conv_1 \times 1 \times 1', 'Conv_3 \times 3 \times 3' and 'Max_pooling_3 \times 3 \times 3' in the original Inception Module, we add two extra operations: 'Conv_1 \times 3 \times 3' and 'Conv_3 \times 1 \times 1' to perform convolution either in spatial or temporal domain only. That is because the size of features in the spatial domain (the height and width of frame) and temporal domain (the number of frames) differ a lot. Consequently, it is not necessary to perform the spatial and temporal convolution together all the time. Besides, a novel operator, dilated convolution 'dil_3 \times 3 \times 3', is introduced into search space for searching more powerful architecture. So the final search space \mathcal{O} we defined includes seven candidate operations: 'Zero', 'Identity', 'dil_3 \times 3 \times 3', 'Conv_1 \times 1 \times 1', 'Conv_3 \times 3 \times 3', 'Conv_1 \times 3 \times 3', 'Conv_3 \times 1 \times 1', where 'Zero' and 'Identity' mean no feature flow connection, direct feature flow without any convolution/pooling operations, respectively. 'Conv_x \times y \times z' and 'dil_x \times y \times z' represent 3D vanilla and dilated convolution that kernel with the size of $x \times y \times z$, respectively. Similar to the work of (Xu et al. 2019), the architecture parameters $\alpha^{(i,j)}$ are optimized via the stochastic mini-batch gradient descent algorithm. Specially, for each edge (i, j) , we can formulate it by a function $o^{(i,j)}(\cdot)$ where $o^{(i,j)}(m_i) = \sum_{o \in \mathcal{O}} \eta_o^{(i,j)} \cdot o(m_i)$. Softmax $\eta_o^{(i,j)} = \frac{\exp(\alpha_o^{(i,j)})}{\sum_{o'' \in \mathcal{O}} \exp(\alpha_{o''}^{(i,j)})}$ is utilized to relax architecture parameter $\alpha^{(i,j)}$ into operation weight $o \in \mathcal{O}$. The intermediate node can be denoted as $m_j = \sum_{i < j} o^{(i,j)}(m_i)$. And the output node m_{k-1} concat all the intermediate nodes. The cross-entropy loss is utilized for the training loss \mathcal{L}_{train} and validation loss \mathcal{L}_{val} . Then the network parameters w and architecture parameters $\alpha^{(i,j)}$ are learned via solving the bi-level optimization problem:

$$\begin{aligned} \min_{\alpha} \quad & \mathcal{L}_{val}(w^*(\alpha), \alpha), \\ \text{s.t.} \quad & w^*(\alpha) = \arg \min_w \mathcal{L}_{train}(w, \alpha) \end{aligned} \quad (1)$$

When the search converging, the optimal operation between the pair of node (i, j) can be obtained by replacing each mixed operation $o^{(i,j)}$ with the most likely operation: $\alpha^{(i,j)} = \arg \max_{o \in \mathcal{O}, o \neq zero} \alpha_o^{(i,j)}$.

Dynamic-static Attention

In the DSA module, two kinds of attention are learned by two sub-modules of dynamic attention and static attention, respectively. In the dynamic attention module, we used our proposed fast approximate rank pooling to learn the motion of gestures, whereas a Gaussian guidance heatmap is learned in the static attention module under the train-phase-only supervision of skeleton data.

Dynamic attention sub-module The dynamic attention sub-module concerns the effective motion information among frames. We aggregate the intermediate spatiotemporal-structural information into a dynamic image instead of using the 3D manipulation directly like (Tran et al. 2015) to avoid time-consuming processing. To improve efficiency, we propose a fast approximate rank pooling algorithm based on (Bilen et al. 2016), and it can reduces time complexity drastically.

Dynamic Image via Fast Approximate Rank Pooling.

According to (Smola and Schölkopf 2004), the rank pooling map can be obtained via solving a convex optimization problem using the objective function of RankSVM. This process is known as rank pooling (Fernando et al. 2017). According to the work(Bilen et al. 2017), the approximation of rank pooling can be defined as:

$$\mathbf{d}^* \propto \sum_{t_1 > t_2} V_{t_1} - V_{t_2} = \sum_{t=1}^T \beta_t V_t, \quad (2)$$

where T is the length of the video clip and $\beta_t = 2t - T - 1$. V_t is the feature map of time step t . The result of Eq.(2) is the dynamic image DI . In this computation, the time complexity is related to the number of frames, for a T -frame video clip, the time consumption can be up to $T(T - 1) \dots 1 = T!$, and it is still high when processing a long-term video.

To simplify the processing of approximating rank pooling, we further study Eq.(2), and achieve the fast approximate rank pooling via computing the relation between the dynamic image of frame n to m ($m > n$) and that of frame $n + 1$ to $m + 1$ as:

$$\begin{aligned} DI(n+1, m+1) = & DI(n, m) + (m - n) \times V(I_n) + \\ & V(I_{m+1}) - 2 \sum_{l=n+1}^m V(I_l) \end{aligned} \quad (3)$$

where I_n is the first frame of last dynamic image, and I_{m+1} is the last frame of the current dynamic image. The last term is the overlapped part between two dynamic images. In this way, the computation of dynamic image can be irrelevant to the number of frames.

After obtaining the dynamic image, at each time t , we do the normalization for the rank parameters as:

$$DI_{\{c,x,y\}} = \frac{DI_{\{c,x,y\}} - DI_{\min}}{DI_{\max} - DI_{\min}}, \quad (4)$$

where $DI_{\{c,x,y\}}$ represents the dynamic image at c -th channel and the coordinate of (x, y) . DI_{\min} and DI_{\max} are the minimum and maximum of the dynamic image, respectively.

Structure of dynamic attention sub-module. Considering the value of dynamic images varies along with the amplitude of movement, which may be out of the range $[0, 1]$. Therefore, we first apply the normalization to the dynamic images. The batch normalization (Ioffe and Szegedy 2015) is conducted to eliminate the influence of distribution inside a mini-batch:

$$DI_{\text{norm}}(t) = \left(\frac{DI(t) - E[DI(t)]}{\sqrt{\text{Var}[DI(t)]}} \right) \times \gamma + \beta, \quad (5)$$

where the expectation E and variance Var are computed over the training data set so that this normalization can consider the data distribution in the mini-batch, γ and β are the scale and shift parameter of the Batch Normalization layer. We add 1 to each pixel of the guidance map to avoid the zero-value attention map, which may lead a vanishing of feature maps. Then we can get the DAtt guided feature map $O_{D,t}^l$ as:

$$O_{D,t}^l = [(DI_{\text{norm}}^l + 1) \odot f_t^l] \otimes f_t^l. \quad (6)$$

where $O_{D,t}^l$ is the guided feature map of layer l at time step t and DI_{norm}^l is dynamic gesture feature map of layer l at time step t . Then, on each channel of the feature map f_t^l , we use the element-wise product operation \odot to generate the attention map. After that, $O_{D,t}^l$ can be derived by the 1×1 convolution of the corresponding attention map and the feature map f_t^l , which we describe with \otimes in Eq.(6). Finally, the shape of $O_{D,t}^l$ is the same as f_t^l .

Structure of the static attention sub-module. Being aware of the location of hands and arms is important to avoid the interference by gesture-irrelevant factors. Therefore, we try to highlight the location of hands/arms in each frame via the static attention sub-module. It is guided by a heatmap, which is related to the location of keypoints in hands/arms regions. The heatmap is derived from a lightweight online gesture region heatmap generation network – HeatmapNet.

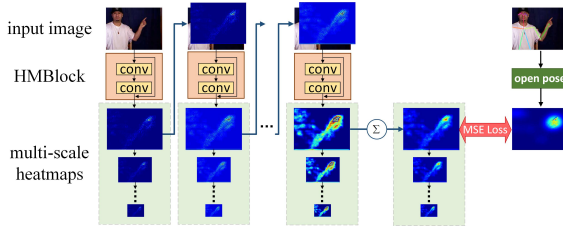


Figure 3: The framework of our HeatmapNet used for guidance heatmap generation. With the Gaussian skeleton map derived via OpenPose (Cao et al. 2017) the ground truth, we learn a heatmap to indicate the hand/arm regions via a lightweight sub-network, which is composed of several cascaded Heatmap Blocks. These blocks can learn a increasingly clear heatmap stage-by-stage.

HeatmapNet. As shown in Fig.3, to derive the ground truth of hands/arms' location, we first employ the OpenPose (Cao et al. 2017) to generate skeleton data from raw RGB videos. Then we obtain the Gaussian skeleton map according to Eq.(7):

$$\mathcal{H}_t = \mathcal{G}(I_t, P_t, \sigma), \quad (7)$$

where I_t and P_t are the input frame and the skeleton points at time t , and its corresponding Gaussian map is represented as \mathcal{H}_t , which is generated via Gaussian function \mathcal{G} with standard deviation σ . After having the Gaussian map as the ground truth, the HeatmapNet is used to learn the static guidance heatmap. Considering the cascaded network is always used in high-level vision tasks (Newell, Yang, and Deng 2016) to learn both global and local cues and refine the details of feature map, we also use a cascaded structure to predict the static guidance map. In each stage of the network, we have a heatmap block (HMBlock) for prediction. The prediction of static guidance map for time step t at stage s can be formulated as:

$$\tilde{h}_t^s = \begin{cases} \mathcal{F}_\theta(I_t) & s = 1 \\ \mathcal{F}_\theta(I_t, \tilde{h}_t^{s-1}) & s > 1, \end{cases} \quad (8)$$

where \mathcal{F}_θ is the residual block with parameter θ . I_t is the input frame at time step t and \tilde{h}_t^{s-1} is the predicted map at the previous stage $s - 1$. With the stage-wise learning of the heatmap, the regions related to the gesture can be highlighted more apparently. Finally, the guidance maps in all the stages are combined by averaging via Eq.(9):

$$h_t = \frac{1}{S} \sum_{s=1}^S \tilde{h}_t^s, \quad (9)$$

where S is the number of stages. To better guide the features of gesture in both low-level and high-level, we then generate multi-scale guidance maps by max pooling. The size of these heatmaps is in accord with those of corresponding feature maps. Then the static guidance maps are fed into different layers of the network to highlight the gesture-relevant regions. Here we use MSE loss \mathcal{L}_{hm}^m to learn the guidance heatmap. It needs to be emphasized that unlike the previous methods (Liu et al. 2017; Wang et al. 2017) based on the detection techniques (*i.e.*, faster R-CNN (Ren et al. 2015)) through the training and test phase, the HeatmapNet is only learned in the training phase, and avoids employing extra input data or complex computation when recognizing gestures. We only use the original skeleton data generated via OpenPose algorithm (Cao et al. 2017) in the training phase, and in the inference phase, we only need to input the original image without additional skeleton information. And our network can automatically focus on the performer's hands and arms. Meanwhile, The FLOPs of our HMBlock is about 5.51×10^8 , whereas that of faster R-CNN is about 36 times of ours at 2.02×10^{10} . Therefore, the addition of HMBlock in the training phase will not increase the burden of learning too much.

Through the SAtt sub-module, we can obtain the guided feature map $O_{S,t}^l$ as Eq. (10):

$$O_{S,t}^l = [(h_t^l + 1) \odot f_t^l] \otimes f_t^l, \quad (10)$$

where $O_{S,t}^l$ is the guided feature map of layer l at time step t and h_t^l is static gesture heatmaps of layer l at time step t . h_t^l is generated via the HeatmapNet. Similar to the dynamic attention sub-module, the processing of "adding 1" to each pixel and the process for shape consistency are also conducted before the element-wise multiplication.

Network Training

The entire network can be trained in an end-to-end manner after overall network architecture is searched out. The main branch of gesture recognition with RGB/depth data is trained together with the branch of HeatmapNet. The parameter of the main branch is learned by minimizing the cross-entropy loss \mathcal{L}_{cls}^m . Meanwhile, the online heatmap sub-network is trained together to learn a guidance heatmap via the MSE loss \mathcal{L}_{hm}^m . Then we jointly optimize the entire network with a multi-task loss function. The Loss function can be expressed as:

$$\begin{aligned} \mathcal{L}^m &= \mathcal{L}_{cls}^m + \gamma \mathcal{L}_{hm}^m \\ &= - \sum_{k=1}^K p_k^m \log(p_k^m) + \gamma \|\mathcal{F}_\theta(I^m) - \mathcal{H}\|^2, \end{aligned} \quad (11)$$

where m indicates the modality of data, which can be either RGB or depth. $p_k = \{p_1, p_2, \dots, p_K\}$ is the ground-truth probability distribution of the k -th class of the gesture, and \hat{p}_k is its estimation. \mathcal{H} is the ground truth Gaussian skeleton map, and $\mathcal{F}_\theta(\cdot)$ is the mapping function the sub-network learning for HMBlocks as mentioned in Section . γ is the balancing parameter and we have $\gamma = 100$ in this paper.

Experiments

Datasets

We evaluate our method and compare it with other state-of-the-art methods on two RGB-D gesture datasets: Chalearn IsoGD dataset (Wan et al. 2016) and NvGesture dataset (Molchanov et al. 2016). Meanwhile, we also conduct the ablation studies on a hand-centred action dataset, THU-READ dataset (Tang et al. 2017, 2018) to show the generality of our network.

Experimental setup

Our experiments are all conducted with Pytorch on the NVIDIA RTX 2080 Ti GPU. During the training process, the inputs are spatially resized to 256×256 and then cropped into 224×224 randomly in the training stage, and are center cropped into 224×224 in the test stage. The data is fed into the network with a mini-batch of 64 samples. For optimization, We use the SGD optimizer to train our network with the weight decay of 0.0003 and the momentum of 0.9. The learning rate is initially fixed as 0.01 and if the accuracy on the validation set not improved every 3 epochs, it is reduced by 10 times. The training work is stopped after 80 epochs or when the learning rate is under 1e-5.

Comparison with state-of-the-art methods

Our method is compared with recent state-of-the-art methods on IsoGD and NvGesture dataset. Table 1 shows the comparison on IsoGD dataset. Since most of methods release their result on the validation subset, we also conduct experiments on it for a fair comparison.

As can be seen in Table 1, our proposed method achieves the best performance on all conditions of using single RGB/depth data and using the fusion of them. For RGB data,

Method	Modality	Accuracy (%)
c-ConvNet (Wang et al. 2018)	RGB	36.60
C3D-gesture <i>et al.</i> (Li et al. 2018)	RGB	37.28
AHL (Hu, Lin, and Hsiu 2018)	RGB	44.88
ResC3D (Li et al. 2017)	RGB	45.07
3DDSN (Duan et al. 2018)	RGB	46.08
3DCNN+LSTM (Zhang et al. 2017)	RGB	51.31
attentionLSTM (Zhang et al. 2018)	RGB	55.98
Redundancy+AttentionLSTM (Zhu et al. 2019)	RGB	57.42
RAAR3DNet(Ours)	RGB	62.66
c-ConvNet (Wang et al. 2018)	Depth	40.08
C3D-gesture (Li et al. 2018)	Depth	40.49
ResC3D (Li et al. 2017)	Depth	48.44
AHL (Hu, Lin, and Hsiu 2018)	Depth	48.96
3DCNN+LSTM (Zhang et al. 2017)	Depth	49.81
attentionLSTM (Zhang et al. 2018)	Depth	53.28
Redundancy+AttentionLSTM (Zhu et al. 2019)	Depth	54.18
3DDSN (Duan et al. 2018)	Depth	54.95
RAAR3DNet(Ours)	Depth	60.66
c-ConvNet (Wang et al. 2018)	RGB-D	44.80
AHL (Hu, Lin, and Hsiu 2018)	RGB-D	54.14
3DCNN+LSTM (Zhang et al. 2017)	RGB-D	55.29
Redundancy+AttentionLSTM (Zhu et al. 2019)	RGB-D	61.05
RAAR3DNet(Ours)	RGB-D	66.62

Table 1: Results on IsoGD dataset.

our method outperforms the second-best one, (Zhu et al. 2019) at about 5%, even though their methods are trained with a complex combination of Res3D, Gated convLSTM and 2D CNNs. Ours is also 17% higher than ResC3D (Li et al. 2017), which achieves 1st place in the 2nd round of Chalearn LAP large-scale isolated gesture recognition challenge. The performance on the depth data is a little lower than that on RGB data. That may because the texture showing the details of fingers is not available in depth data. However, the recognition result on depth data is similar to that on RGB data. Ours also outperform the second-best one, 3DDSN (Duan et al. 2018) about 6%. The performance on the fusion RGB-D data also shows the effectiveness of our method, which outperforms Zhu *et al.*'s method at about 5.6%.

The comparison on NvGesture dataset is shown in Table 2. As can be seen, our method can still achieve a competitive result on this dataset. Compared with the method of MTUT *et al.* (Molchanov et al. 2016), which uses a combination of time-consuming models of C3D and LSTM, our network achieves about 4.5% improvement on RGB data. Meanwhile, it outperforms GPM (Gupta et al. 2019), the second-best result on depth data at about 1.17%. The gap between the performance of ours and GPM becomes more significant on the fusion of RGB-D data at 2.49%. Noticing that our result is also better than the human recognition accuracy even without auxiliary data like IR as provided in that dataset. It shows the effectiveness of our network architecture searching strategy and the attention module for improving the recognition performance.

Ablation studies

In this section, we perform several groups of experiments to verify the effect of each component of our network, including the idea of automatically searching the architecture of network and the spatiotemporal DSA module.

Method	Modality	Accuracy (%)
HOG+HOG ² (Ohn-Bar and Trivedi 2014)	RGB	24.50
Simonyan <i>et al.</i> (Simonyan and Zisserman 2014)	RGB	54.60
Wang <i>et al.</i> (Wang et al. 2016a)	RGB	59.10
C3D (Tran et al. 2015)	RGB	69.30
R3DCNN (Molchanov et al. 2016)	RGB	74.10
GPM (Gupta et al. 2019)	RGB	75.90
PreRNN (Yang, Molchanov, and Kautz 2018)	RGB	76.50
ResNeXt-101 (Köpüklü et al. 2019)	RGB	78.63
MTUT (Abavisan, Joze, and Patel 2019)	RGB	81.33
RAAR3DNet(Ours)	RGB	85.83
HOG+HOG ² (Ohn-Bar and Trivedi 2014)	Depth	36.30
SNV (Yang and Tian 2014)	Depth	70.70
C3D (Tran et al. 2015)	Depth	78.80
R3DCNN (Molchanov et al. 2016)	Depth	80.30
ResNeXt-101 (Köpüklü et al. 2019)	Depth	83.82
PreRNN (Yang, Molchanov, and Kautz 2018)	Depth	84.40
MTUT (Abavisan, Joze, and Patel 2019)	Depth	84.85
GPM (Gupta et al. 2019)	Depth	85.50
RAAR3DNet(Ours)	Depth	86.67
HOG+HOG ² (Ohn-Bar and Trivedi 2014)	RGB-D	36.90
I3D (Carreira and Zisserman 2017)	RGB-D	83.82
PreRNN (Yang, Molchanov, and Kautz 2018)	RGB-D	85.00
MTUT (Abavisan, Joze, and Patel 2019)	RGB-D	85.48
GPM (Gupta et al. 2019)	RGB-D	86.10
human		88.4
RAAR3DNet(Ours)	RGB-D	88.59

Table 2: Results on the NvGesture dataset.

Effect of network architecture searching. Here we first compare the performance of the baseline raw I3D network and our proposed network on three different datasets - IsoGD, NvGesture and THU-READ dataset.

Dataset	Network	I3D		RAAR3DNet (w/o DSA)	
		RGB	Depth	RGB	Depth
IsoGD		59.15%	56.64%	61.13%	58.32 %
NvGesture		81.67%	83.12%	82.50%	85.83%
THU-READ		65.5%	67.5%	67.92%	68.75%

Table 3: Comparisons with raw I3D and RAAR3DNet on the Gesture and Action dataset.

As shown in Table 3, with a sophisticated network structure that searched via NAS, the performance on three datasets can be about 1% higher than the original I3D network on RGB data and about 2% higher on depth data. To better illustrate the effect of architecture searching, we also visualize the features of the original I3D network and those of the reconstructed network in Fig.4. From the visualization result we can clearly find that via searching the optimal structure of network, the response of the background and other gesture-irrelevant regions in the feature maps is decreased significantly. It shows that searching and reconstructing the internal structure of a network architecture can make it more suitable for the specific task and extract more reasonable features.

Effect of attention mechanism. Table 4 shows the influence of different attention schemes. For a fair comparison, we remove other modules and only take the original I3D network as the baseline. We give the result of the original I3D, the network only with dynamic attention or static attention, and finally the entire DSA module.

As shown in Table 4, the DSA module can improve the

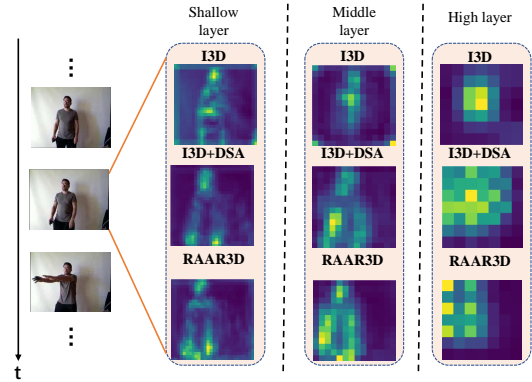


Figure 4: Visualization of feature maps in the early, middle and late stage of the network. The feature maps from top to bottom are with the I3D, I3D with DSA module and our ultimate RAAR3D network, respectively.

Strategy	Recognition Rate	
	RGB	Depth
baseline(I3D)	81.67%	83.12%
DAtt	83.54%	84.58%
SAtt	83.75%	85.21%
DSA(DAtt+SAtt)	84.79%	85.83%

DAtt = dynamic attention, SAtt = static attention

Table 4: Performance of attention modules on the NVGesture dataset.

performance at about 3% on the basic I3D network, which implies the attention mechanism plays a very important role in the video-based recognition tasks since it can help the network to focus on the most noteworthy regions. Compared with the dynamic attention sub-module, the gain brought by static attention is a little higher. The reason for it may be the details of hands/arms is more important for recognizing some subtle differences. Therefore, the highlight of regions of hands/arms contributes more to the improvement.

Conclusion

In this paper, we propose a regional attention with searched architecture 3D network for gesture recognition basing on RGB-D data. We take the I3D network as the backbone, and employ NAS to search the optimal connection among features in different stages of it. In this way, the structure of the network can fit the low-level and high-level features better and improves the recognition result. Meanwhile, we also design a stackable attention module of DSA to guide the network to pay more attention to the hand/arm regions in each frame and the motion trajectory among video sequence. Finally, comparisons with state-of-the-art methods on two gesture datasets prove the effectiveness of the proposed method.

Acknowledgement

This work was supported by the National Key R&D Program of China under Grant #2018YFC0807500, the Chinese National Natural Science Foundation Projects #61961160704, #61876179, #62002271, #61772396, #61772392, #61902296, the Fundamental Research Funds for the Central Universities #JBF180301, Xi'an Key Laboratory of Big Data and Intelligent Vision #201805053ZD4CG37, the External cooperation key project of Chinese Academy Sciences #173211KYSB20200002, the Key Project of the General Logistics Department Grant No.ASW17C001, Science and Technology Development Fund of Macau (No. 0019/2018/ASC, 0010/2019/AFJ, 0025/2019/AKP).

References

Abavisani, M.; Jozé, H. R. V.; and Patel, V. M. 2019. Improving the performance of unimodal dynamic hand-gesture recognition with multimodal training. In *CVPR*, 1165–1174.

Bilen, H.; Fernando, B.; Gavves, E.; and Vedaldi, A. 2017. Action recognition with dynamic image networks. *TPAMI* .

Bilen, H.; Fernando, B.; Gavves, E.; Vedaldi, A.; and Gould, S. 2016. Dynamic image networks for action recognition. In *CVPR*, 3034–3042.

Cao, Z.; Simon, T.; Wei, S.-E.; and Sheikh, Y. 2017. Re-altime Multi-Person 2D Pose Estimation using Part Affinity Fields. In *CVPR*.

Carreira, J.; and Zisserman, A. 2017. Quo vadis, action recognition? a new model and the kinetics dataset. In *CVPR*, 4724–4733. IEEE.

Chu, X.; Yang, W.; Ouyang, W.; Ma, C.; Yuille, A. L.; and Wang, X. 2017. Multi-context attention for human pose estimation. In *CVPR*, 1831–1840.

Cui, R.; Liu, H.; and Zhang, C. 2019. A deep neural framework for continuous sign language recognition by iterative training. *IEEE TMM* 21(7): 1880–1891.

Duan, J.; Wan, J.; Zhou, S.; Guo, X.; and Li, S. Z. 2018. A unified framework for multi-modal isolated gesture recognition. *TOMM* 14(1): 21.

Fernando, B.; Gavves, E.; Oramas, J.; Ghodrati, A.; and Tuytelaars, T. 2017. Rank pooling for action recognition. *TPAMI* 39(4): 773–787.

Gupta, V.; Dwivedi, S. K.; Dabral, R.; and Jain, A. 2019. Progression Modelling for Online and Early Gesture Detection. In *3DV*, 289–297. IEEE.

He, K.; Zhang, X.; Ren, S.; and Sun, J. 2016. Deep residual learning for image recognition. In *CVPR*, 770–778.

Hu, J.; Shen, L.; and Sun, G. 2018. Squeeze-and-excitation networks. In *CVPR*, 7132–7141.

Hu, T.-K.; Lin, Y.-Y.; and Hsiu, P.-C. 2018. Learning Adaptive Hidden Layers for Mobile Gesture Recognition. In *AAAI*, 6934–6942.

Ioffe, S.; and Szegedy, C. 2015. Batch normalization: Accelerating deep network training by reducing internal covariate shift. In *ICML*, 448–456.

Karpathy, A.; Toderici, G.; Shetty, S.; Leung, T.; Sukthankar, R.; and Fei-Fei, L. 2014. Large-scale video classification with convolutional neural networks. In *CVPR*, 1725–1732.

Klaser, A.; Marszałek, M.; and Schmid, C. 2008. A spatio-temporal descriptor based on 3d-gradients. In *BMVC*, 1–10.

Köpüklü, O.; Gunduz, A.; Kose, N.; and Rigoll, G. 2019. Real-time hand gesture detection and classification using convolutional neural networks. In *FG*, 1–8. IEEE.

Li, H.; Liu, Y.; Ouyang, W.; and Wang, X. 2019a. Zoom out-and-in network with map attention decision for region proposal and object detection. *IJCV* 127(3): 225–238.

Li, Y.; Miao, Q.; Ouyang, W.; Ma, Z.; Fang, H.; Dong, C.; and Quan, Y. 2019b. LAP-Net: Level-Aware Progressive Network for Image Dehazing. In *ICCV*, 3276–3285.

Li, Y.; Miao, Q.; Tian, K.; Fan, Y.; Xu, X.; Li, R.; and Song, J. 2016. Large-scale gesture recognition with a fusion of RGB-D data based on the C3D model. In *ICPR*, 25–30. IEEE.

Li, Y.; Miao, Q.; Tian, K.; Fan, Y.; Xu, X.; Li, R.; and Song, J. 2018. Large-scale gesture recognition with a fusion of RGB-D data based on saliency theory and C3D model. *TCSVT* 28(10): 2956–2964.

Li, Y.; Miao, Q.; Tian, K.; Fan, Y.; Xu, X.; Ma, Z.; and Song, J. 2017. Large-scale Gesture Recognition with a Fusion of RGB-D Data Based on Optical Flow and the C3D Model. *PRL* .

Li, Y.; Wan, J.; Miao, Q.; Escalera, S.; Fang, H.; Chen, H.; Qi, X.; and Guo, G. 2020. CR-Net: A Deep Classification-Regression Network for Multimodal Apparent Personality Analysis. *IJCV* 1–18.

Lin, C.; Wan, J.; Liang, Y.; and Li, S. Z. 2018. Large-Scale Isolated Gesture Recognition Using a Refined Fused Model Based on Masked Res-C3D Network and Skeleton LSTM. In *FG*, 52–58. IEEE.

Liu, H.; Simonyan, K.; and Yang, Y. 2019. Darts: Differentiable architecture search. *ICLR* .

Liu, Z.; Chai, X.; Liu, Z.; and Chen, X. 2017. Continuous gesture recognition with hand-oriented spatiotemporal feature. In *Proceedings of the IEEE International Conference on Computer Vision Workshops*, 3056–3064.

Miao, Q.; Li, Y.; Ouyang, W.; Ma, Z.; Xu, X.; Shi, W.; and Cao, X. 2017. Multimodal Gesture Recognition Based on the ResC3D Network. In *ICCVWorkshops*, 3047–3055.

Molchanov, P.; Yang, X.; Gupta, S.; Kim, K.; Tyree, S.; and Kautz, J. 2016. Online Detection and Classification of Dynamic Hand Gestures With Recurrent 3D Convolutional Neural Network. In *CVPR*, 4207–4215. IEEE.

Narayana, P.; Beveridge, R.; and Draper, B. A. 2018. Gesture recognition: Focus on the hands. In *CVPR*, 5235–5244.

Newell, A.; Yang, K.; and Deng, J. 2016. Stacked hourglass networks for human pose estimation. In *ECCV*, 483–499.

Ohn-Bar, E.; and Trivedi, M. M. 2014. Hand gesture recognition in real time for automotive interfaces: A multimodal vision-based approach and evaluations. *IEEE transactions on intelligent transportation systems* 15(6): 2368–2377.

Peng, W.; Hong, X.; and Zhao, G. 2019. Video Action Recognition Via Neural Architecture Searching. In *ICIP*, 11–15.

Pérez-Rúa, J.-M.; Vielzeuf, V.; Pateux, S.; Baccouche, M.; and Jurie, F. 2019. Mfas: Multimodal fusion architecture search. In *CVPR*, 6966–6975.

Qiu, Z.; Yao, T.; and Mei, T. 2017. Learning spatio-temporal representation with pseudo-3d residual networks. In *ICCV*, 5534–5542. IEEE.

Real, E.; Aggarwal, A.; Huang, Y.; and Le, Q. V. 2019. Regularized evolution for image classifier architecture search. In *AAAI*, volume 33, 4780–4789.

Real, E.; Moore, S.; Selle, A.; Saxena, S.; Suematsu, Y. L.; Tan, J.; Le, Q. V.; and Kurakin, A. 2017. Large-scale evolution of image classifiers. In *ICML*, 2902–2911.

Ren, S.; He, K.; Girshick, R.; and Sun, J. 2015. Faster R-CNN: Towards real-time object detection with region proposal networks. In *NIPS*, 91–99.

Simonyan, K.; and Zisserman, A. 2014. Two-stream convolutional networks for action recognition in videos. In *NIPS*, 568–576.

Smola, A. J.; and Schölkopf, B. 2004. A tutorial on support vector regression. *Statistics and computing* 14(3): 199–222.

Tang, Y.; Tian, Y.; Lu, J.; Feng, J.; and Zhou, J. 2017. Action recognition in rgb-d egocentric videos. In *ICIP*, 3410–3414.

Tang, Y.; Wang, Z.; Lu, J.; Feng, J.; and Zhou, J. 2018. Multi-stream deep neural networks for rgb-d egocentric action recognition. *IEEE TCSVT* 29(10): 3001–3015.

Tran, D.; Bourdev, L.; Fergus, R.; Torresani, L.; and Paluri, M. 2015. Learning spatiotemporal features with 3d convolutional networks. In *ICCV*, 4489–4497. IEEE.

Wan, J.; Guo, G.; and Li, S. 2015. Explore Efficient Local Features from RGB-D Data for One-shot Learning Gesture Recognition. *TPAMI* 38(8): 1626–1639.

Wan, J.; Ruan, Q.; Li, W.; An, G.; and Zhao, R. 2014. 3D SMoSIFT: three-dimensional sparse motion scale invariant feature transform for activity recognition from RGB-D videos. *Journal of Electronic Imaging* 23(2): 3017–3017.

Wan, J.; Zhao, Y.; Zhou, S.; Guyon, I.; Escalera, S.; and Li, S. Z. 2016. Chalearn looking at people rgb-d isolated and continuous datasets for gesture recognition. In *CVPRWorkshops*, 56–64.

Wang, H.; Oneata, D.; Verbeek, J.; and Schmid, C. 2016a. A robust and efficient video representation for action recognition. *IJCV* 119(3): 219–238.

Wang, H.; Wang, P.; Song, Z.; and Li, W. 2017. Large-Scale Multimodal Gesture Segmentation and Recognition Based on Convolutional Neural Networks. In *ICCV*, 3138–3146.

Wang, P.; Li, W.; Liu, S.; Gao, Z.; Tang, C.; and Ogunbona, P. 2016b. Large-scale isolated gesture recognition using convolutional neural networks. In *ICPR*, 7–12. IEEE.

Wang, P.; Li, W.; Liu, S.; Zhang, Y.; Gao, Z.; and Ogunbona, P. 2016c. Large-scale continuous gesture recognition using convolutional neural networks. In *ICPR*, 13–18. IEEE.

Wang, P.; Li, W.; Wan, J.; Ogunbona, P.; and Liu, X. 2018. Cooperative Training of Deep Aggregation Networks for RGB-D Action Recognition. In *AAAI*.

Wang, X.; Xiong, X.; Neumann, M.; Piergiovanni, A.; Ryoo, M. S.; Angelova, A.; Kitani, K. M.; and Hua, W. 2020. AttentionNAS: Spatiotemporal Attention Cell Search for Video Classification. *arXiv preprint arXiv:2007.12034*.

Xu, Y.; Xie, L.; Zhang, X.; Chen, X.; Qi, G.-J.; Tian, Q.; and Xiong, H. 2019. PC-DARTS: Partial Channel Connections for Memory-Efficient Architecture Search. In *ICLR*.

Yang, X.; Molchanov, P.; and Kautz, J. 2018. Making convolutional networks recurrent for visual sequence learning. In *CVPR*, 6469–6478.

Yang, X.; and Tian, Y. 2014. Super normal vector for activity recognition using depth sequences. In *CVPR*, 804–811.

Yu, Z.; Zhou, B.; Wan, J.; Wang, P.; Chen, H.; Liu, X.; Li, S. Z.; and Zhao, G. 2020. Searching Multi-Rate and Multi-Modal Temporal Enhanced Networks for Gesture Recognition. *arXiv preprint arXiv:2008.09412*.

Zhang, H.; Hou, Y.; Wang, P.; Guo, Z.; and Li, W. 2020. SAR-NAS: Skeleton-based action recognition via neural architecture searching. *Journal of Visual Communication and Image Representation* 73: 102942.

Zhang, L.; Zhu, G.; Mei, L.; Shen, P.; Shah, S. A. A.; and Bennamoun, M. 2018. Attention in convolutional LSTM for gesture recognition. In *NIPS*, 1953–1962.

Zhang, L.; Zhu, G.; Shen, P.; Song, J.; Shah, S. A.; and Bennamoun, M. 2017. Learning Spatiotemporal Features Using 3DCNN and Convolutional LSTM for Gesture Recognition. In *ICCV*, 3120–3128.

Zhu, G.; Zhang, L.; Shen, P.; and Song, J. 2017. Multimodal Gesture Recognition Using 3D Convolution and Convolutional LSTM. *IEEE Access* 5: 4517–4524.

Zhu, G.; Zhang, L.; Yang, L.; Mei, L.; Shah, S. A. A.; Bennamoun, M.; and Shen, P. 2019. Redundancy and Attention in Convolutional LSTM for Gesture Recognition. *TNNLS* 31(4): 1323–1335.

Zoph, B.; Vasudevan, V.; Shlens, J.; and Le, Q. V. 2018. Learning transferable architectures for scalable image recognition. In *CVPR*, 8697–8710.